Report No.
UCB/SEMM-2011/03

Structural Engineering
Mechanics and Materials

Backside Feature Transfer during Electrostatic Chucking

By

Gerd Brandstetter

February 2011

Department of Civil and Environmental Engineering
University of California, Berkeley

Preface

This work was done as Master Thesis in order to fulfill the Master of Science in Mechanical Engineering degree requirement at ETH Zurich, Switzerland. It has been carried out under the supervision of Professor Sanjay Govindjee at the University of California in Berkeley, USA. I would like to thank Professor Govindjee for his extraordinary support and help and the opportunity to work on such a nice analysis project.

Berkeley, February 2009

Gerd Brandstetter

Contents

List of Figures

Abstract

During electrostatic chucking of a reticle, non-flatness features of the clamped backside surface are flattened out and transmitted to the frontside. To predict the reticle deformation one could use the finite element method. However these computations are time consuming, especially when a fine mesh is needed to account for sharp changes in surface shapes. So far no analytical description has been carried out on the behavior of how backside non-flatness features are transmitted to the frontside. It is the purpose of this thesis to develop a theory in two and three dimensions that allows to estimate the magnitude of the transferred spectral components of a regular backsurface shape. Mainly two observations have been made. First, the reticle itself is acting as a low-pass filter: Components of high spatial frequencies in the backside non-flatness are damped out and cannot be seen at the frontside after chucking. Second, the applied voltage on an electrostatic chuck imposes a limit on the backside non-flatness magnitude that can be flattened out, depending on its wavelength. Results are compared to finite element calculations and show good agreement.

1 Introduction

In semiconductor fabrication an important process is the pattern transfer from a mask to the waver by electromagnetic waves. The schematic of this called lithography can be seen in Figure 1. Next generation extreme ultraviolet lithography requires a very low image placement error and hence a strict error tolerance in mask flatness and in-plane distortion. Magnitudes of typical distortions are in a micrometer to nanometer range. Due to these error tolerances and the small wavelength of the light used to write the wafer, the whole process takes place in vacuum. Typically the mask is held by an electrostatic chuck which implies a clamping pressure due to the electrical field between chuck electrodes and conducting reticle back side. In Figure 2 we see a schematic of a bipolar chuck with the reticle below. Without loss of generality, one can assume a perfectly flat chuck and reticle frontside surface. The question in this report is, how a regular backsurface shape gets flattened out at a certain voltage applied on the chuck, and what the frontside look like after electrostatic chucking (called e-chucking from now on). This allows one to predict the frontside displacement of the chucked reticle at a certain voltage, given the backside surface shape before the e-chucking process.

Outline of the Report

At first we focus on the two dimensional case. To predict the removal of a periodic non-flatness on the backside, we deal with the reverse case where we apply a periodic boundary condition on a perfectly flat backside surface and ask how much of this displacement is transferred to the frontside. This is possible due to the small displacements/strains which allows us to treat the system as linear elastic. Solving this problem is called ideal flattening in this context. Here we already observe the two main properties of feature transfers. Namely the frequency dependance of the transmitted waves' amplitudes as well as the correlation between the magnitude of loading and resulting displacement.

Knowing the exact solution of ideal flattening in two dimensions, we can compare it to the result of an asymptotic approximation method. As expected this leads to the same solution when using proper ansatz functions. The three dimensional case of ideal flattening will be solved by applying this same approximation technique.

In order to understand the behavior of real e-chucking, we introduce the ideal e-chucking model. This allows us to define a connection between the boundary conditions of ideal flattening and those resulting from a two body chuck-reticle contact problem when applying a certain voltage on a bipolar chuck. As a result we get the so called coefficient of transmission and an estimate on the maximum allowable amplitude of a harmonic backside displacement that can be flattened at a certain voltage. Both depend on the wavelength of the backside perturbation. This defines a filter for the transmission of spectral components of a regular backsurface shape. After performing a discrete cosine transformation of an exemplary reticle backsurface shape and applying the derived filter method, the inverse transformation gives the actual frontside surface shape at a certain voltage.

In the end we test and compare this theory in two and three dimensions to a finite element

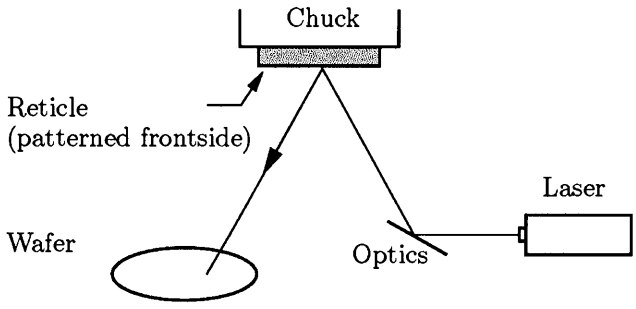

Figure 1: Schematic of lithography.

analysis of a real e-chucking model. There is a good agreement between the analytical and finite element calculation observed, especially for higher spatial frequency perturbations.

Used Software

Analytical computations have been carried out partly as hand-calculations, partly using the Mathematica ® software. Numerical computations and resulting plots have been done in Matlab ®. For the finite element analysis the software FEAP ® is used which is licensed and distributed by the University of California.

Terminology

There is a glossary appended where the most important terms used are defined.

Numerical Data

For the illustration of the derived theoretical results and a verification by finite element analysis, typical reticle geometries and material properties are used as found in literature (e.g. [3]). To give an example of an arbitrary reticle backsurface shape in the end of Chapter 3 and 4, we apply a spline approximation of random numbers generated by Matlab. The implementation of the spline routine, which is also used for the mesh generation in FEAP, is based on the algorithm as outlined in Appendix A.

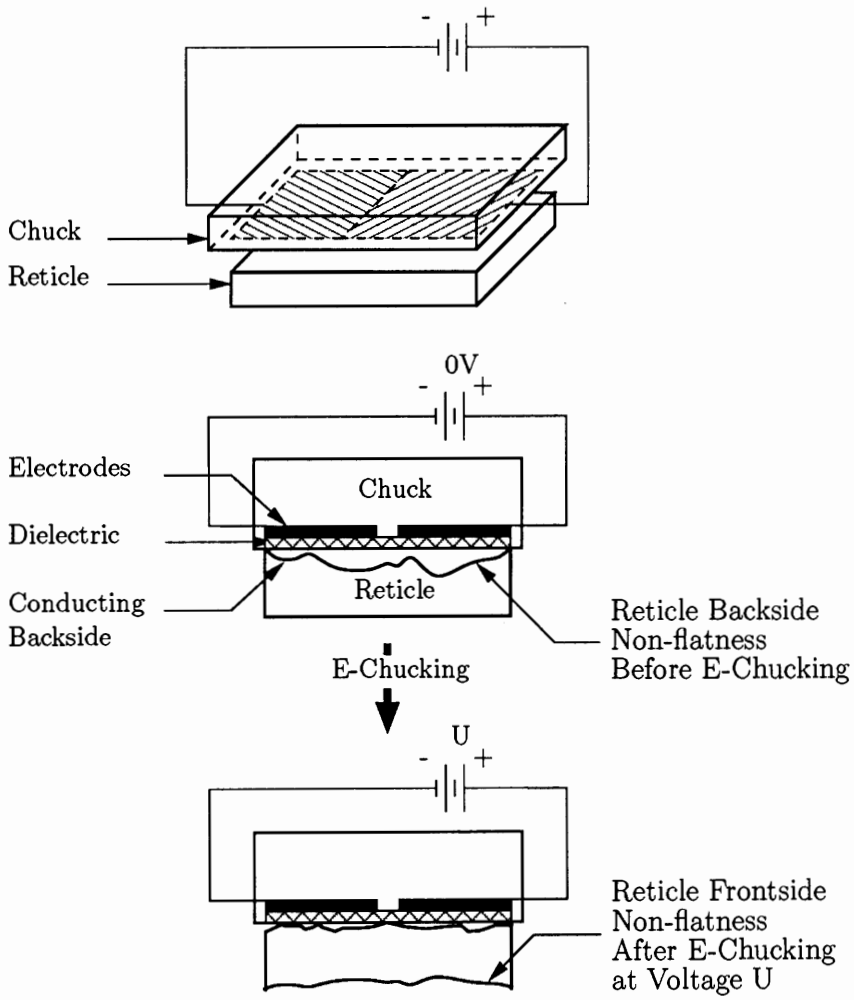

Figure 2: Overview e-chucking process.

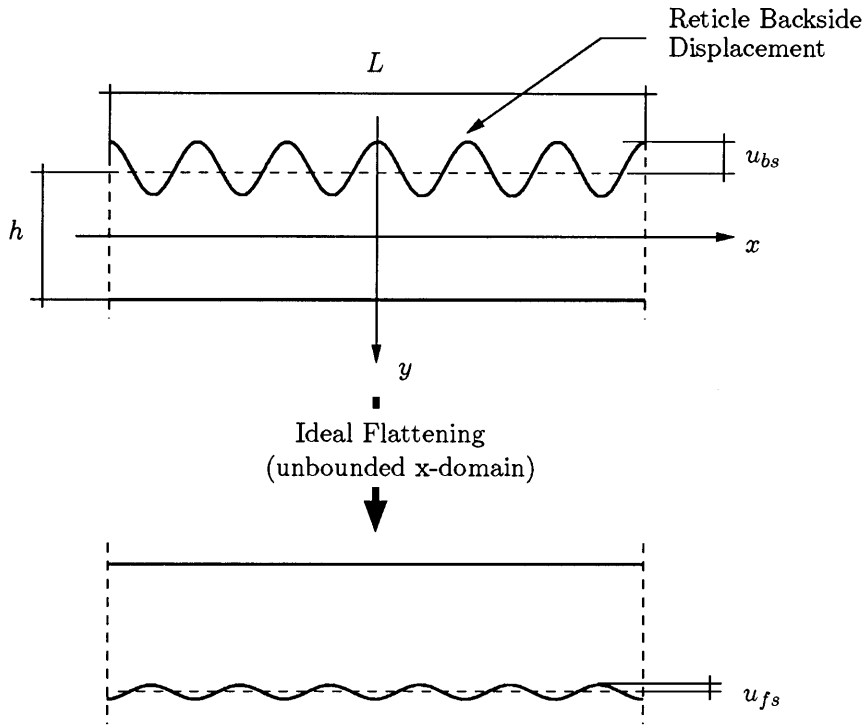

Figure 3: Two dimensional idealization of reticle geometry before and after ideal flattening (unbounded x-domain).

2 Two Dimensional Ideal Flattening

Consider the reticle geometry shown in Figure 3, where the length L will later be taken as 152 mm and the reticle thickness h will later be taken as 6.35 mm. In a first step we will treat the reticle as unbounded in the x-direction and only bounded in y-direction by h. This allows us to initially avoid edge effects which are analyzed in the end of this chapter. As ideal flattening we refer to the model, where we apply a harmonic pressure on the reticle backside and ask for the resulting deformation. After developing the analytical exact solution of this problem, we test an approximation method which is used for the three dimensional analysis as well. As one result we get the transmission coefficient, which is defined to be the ratio u_{fs}/u_{bs} (see Figure 3).

2.1 Analytical Solution (Unbounded x-Domain)

Let us begin with an infinitely large reticle in the x-direction and thickness h in y-direction. On the backside, $y = -h/2$, we will assume a friction free clamping with n waves over the span L. This corresponds to assuming a feature wavelength $\lambda = L/n$. Although L does not bound our domain of interest yet, we introduce it here as a periodic domain of the infinitely

large reticle. Due to linearity, we know that we will have to impose a (self-equilibrated) normal traction on this surface with the same wavelength. Given that all the other surfaces are traction free, we find that we need to solve the classical elasticity problem with the following boundary conditions:

$$\begin{aligned} \sigma_{yy}(x, h/2) &= 0 && (2.1)\\ \sigma_{yx}(x, h/2) &= 0 && (2.2)\\ \sigma_{yy}(x, -h/2) &= A\cos(\alpha x) && (2.3)\\ \sigma_{yx}(x, -h/2) &= 0 && (2.4) \end{aligned}$$

where $\alpha = 2n\pi/L$ and $n = 1, 2, \ldots$ is called the wavenumber in this context. A is the unknown magnitude of the surface traction needed to effect the imposed displacement.

This classical problem can be solved by using a Levy expansion of the Airy stress function as outlined in [5, Art. 24]. For the problem at hand, we can assume that the Airy stress function has the following form:

$$\phi(x, y) = \cos(\alpha x) f(y)\,, \tag{2.5}$$

where $f(y)$ is unknown. The stress function must satisfy the bi-harmonic equation $\nabla^4\phi = 0$. This implies that the function $f(\cdot)$ satisfies the ordinary differential equation

$$f'''' - 2\alpha^2 f'' + \alpha^4 f = 0\,. \tag{2.6}$$

Using variation of parameters, it can be shown that

$$f(y) = C_1\cosh(y) + C_2\sinh(y) + C_3 y\cosh(y) + C_4 y\sinh(y)\,, \tag{2.7}$$

where C_i are constants of integration which are determined from the stress boundary conditions by noting that $\sigma_{xx} = \phi_{,yy}$, $\sigma_{yy} = \phi_{,xx}$, and $\sigma_{xy} = -\phi_{,xy}$. Applying our boundary conditions and the relations between the stress function and the stresses, allows us to write the stress field as

$$\begin{aligned} \sigma_{xx} &= A\cos(\alpha x)\left\{\cosh(\alpha y)\left[K_1 + yK_3\right] - \sinh(\alpha y)\left[K_2 + yK_4\right]\right\} && (2.8)\\ \sigma_{yy} &= A\cos(\alpha x)\left\{-\cosh(\alpha y)\left[\bar{K}_1 + yK_3\right] + \sinh(\alpha y)\left[\bar{K}_2 + yK_4\right]\right\} && (2.9)\\ \sigma_{xy} &= A\sin(\alpha x)\left\{-\cosh(\alpha y)\left[K_5 + yK_4\right] + \sinh(\alpha y)\left[K_6 + yK_3\right]\right\}\,, && (2.10) \end{aligned}$$

where the constants K_i are given as

$$K_1 = \frac{\sinh(\frac{\alpha h}{2}) - \frac{\alpha h}{2}\cosh(\frac{\alpha h}{2})}{\sinh(\alpha h) + \alpha h} \tag{2.11}$$

$$K_2 = \frac{\cosh(\frac{\alpha h}{2}) - \frac{\alpha h}{2}\sinh(\frac{\alpha h}{2})}{\sinh(\alpha h) - \alpha h} \tag{2.12}$$

$$K_3 = -\frac{\alpha\cosh(\frac{\alpha h}{2})}{\sinh(\alpha h) - \alpha h} \tag{2.13}$$

$$K_4 = -\frac{\alpha\sinh(\frac{\alpha h}{2})}{\sinh(\alpha h) + \alpha h} \tag{2.14}$$

$$\bar{K}_1 = K_1 + \frac{2}{\alpha}K_4 \tag{2.15}$$

$$\bar{K}_2 = K_2 + \frac{2}{\alpha}K_3 \tag{2.16}$$

$$K_5 = \frac{1}{2}(K_2 + \bar{K}_2) \tag{2.17}$$

$$K_6 = \frac{1}{2}(K_1 + \bar{K}_1)\,. \tag{2.18}$$

Note that this stress field exactly satisfies the given boundary conditions.

With the stress field known we can find the strain field using the linear elastic constitutive relation. For isotropic materials we have that

$$\varepsilon_{xx} = \frac{1}{E}(\sigma_{xx} - \nu\sigma_{yy}) \tag{2.19}$$

$$\varepsilon_{yy} = \frac{1}{E}(\sigma_{yy} - \nu\sigma_{xx}) \tag{2.20}$$

$$2\varepsilon_{xy} = \frac{2(1+\nu)}{E}\sigma_{xy}\,, \tag{2.21}$$

where E is the Young's modulus and ν Poisson's ratio. If one wishes to examine a plane strain model as opposed to a generalized plane stress model, then one needs to replace E by

$$\bar{E} = E/(1-\nu^2) \tag{2.22}$$

and ν by

$$\bar{\nu} = \nu/(1-\nu)\,; \tag{2.23}$$

i.e. one needs to use the plane strain moduli. The strains are the symmetric gradient components of the displacement field; thus the displacement field can be found by integrating

the strain expressions. Upon integration and removal of the rigid body modes one finds

$$u_x = \frac{A}{\alpha \bar{E}} \sin(\alpha x) \left\{ \cosh(\alpha y) \left[K_1 + \bar{\nu}\bar{K}_1 + y(1+\bar{\nu})K_3 \right] - \sinh(\alpha y) \left[K_2 + \bar{\nu}\bar{K}_2 + y(1+\bar{\nu})K_4 \right] \right\} \tag{2.24}$$

$$u_y = \frac{A}{\alpha \bar{E}} \cos(\alpha x) \left\{ \cosh(\alpha y) \left[\frac{1+\bar{\nu}}{\alpha} K_3 + \bar{\nu}K_2 + \bar{K}_2 + y(1+\bar{\nu})K_4 \right] - \sinh(\alpha y) \left[\frac{1+\bar{\nu}}{\alpha} K_4 + \bar{\nu}K_1 + \bar{K}_1 + y(1+\bar{\nu})K_3 \right] \right\} . \tag{2.25}$$

Note that these equations are found by integration of the normal strain relations in the x- and y-directions and they are fully consistent with the shear strain equation. For later analysis we define the amplitudes

$$u_{bs} := |u_y(x=0, y=-h/2)| \tag{2.26}$$

$$u_{fs} := |u_y(x=0, y=h/2)| . \tag{2.27}$$

Of primal interest to us is the transmission coefficient $c_T = u_{fs}/u_{bs}$. From our solution we find that

$$c_{T,2d} = \frac{u_y(x, h/2)}{u_y(x, -h/2)} = \frac{2(\alpha h \cosh(\alpha h) + \sinh(\alpha h))}{2\alpha h + \sinh(2\alpha h)} . \tag{2.28}$$

By setting $d = h/L$ the trend for varying wavenumbers and thickness-to-length ratios can be seen in Figure 4. The case where $d = 0.0418$ corresponds to a reticle length of 152 mm and 6.35 mm thickness.

2.2 Asymptotic Approximation via Minimization of Potential Energy

In the three dimensional case we will derive the solution via energy minimization. To test this method we apply it here in two dimensions where we know the exact solution. A comparison will show that this approximation gives the exact solution when choosing appropriate ansatz functions.

First one needs to choose the ansatz functions for the displacement field. Let us assume:

$$u_y = \cos(\alpha x) \cdot (C_1 \cosh(\alpha y) + C_2 \sinh(\alpha y) + C_3 y \cosh(\alpha y) + C_4 y \sinh(\alpha y)) \tag{2.29}$$

$$u_x = \sin(\alpha x) \cdot (C_5 \cosh(\alpha y) + C_6 \sinh(\alpha y) + C_7 y \cosh(\alpha y) + C_8 y \sinh(\alpha y)) . \tag{2.30}$$

The strain tensor field ϵ is then given by

$$\epsilon_{ij} = \frac{1}{2}(u_{i,j} + u_{j,i}) , \tag{2.31}$$

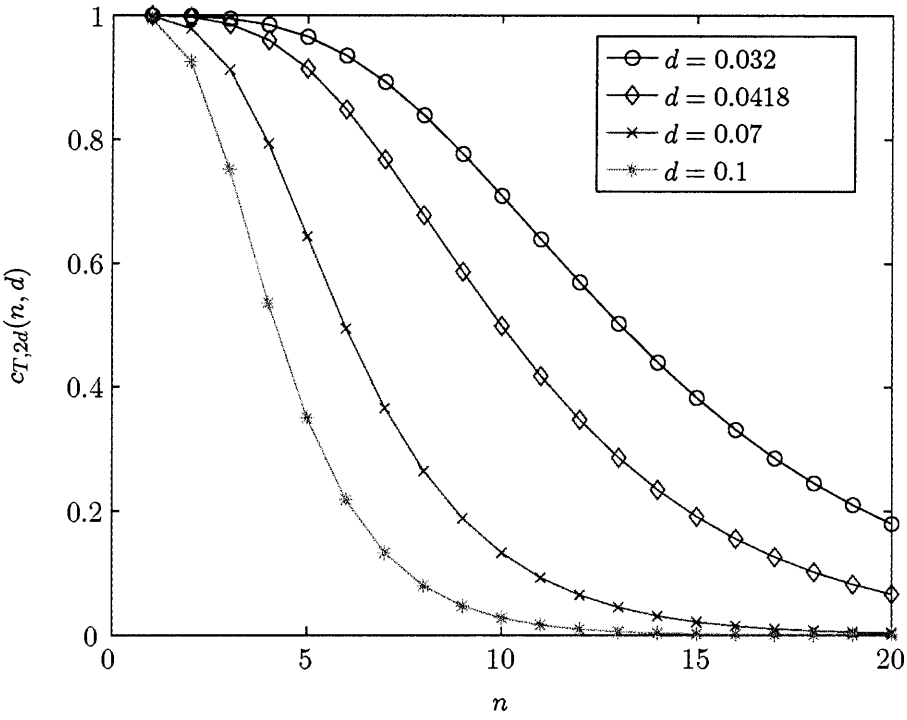

Figure 4: Analytical transmission coefficient in two dimensions.

where $i, j \in (x, y)$. The Lame-parameters for the plane strain case are given by

$$\bar{\mu} = \frac{\bar{E}}{2(1+\bar{\nu})} \tag{2.32}$$

$$\bar{\lambda} = \frac{\bar{\nu}\bar{E}}{(1-2\bar{\nu})(1+\bar{\nu})}\,. \tag{2.33}$$

Then the stress field σ can be computed by

$$\sigma_{ij} = 2\bar{\mu}\epsilon_{ij} + \bar{\lambda}\delta_{ij}\epsilon_{kk}\,, \tag{2.34}$$

where δ_{ij} is the Kronecker-Delta and equals one if $i = j$ and zero else. Let us focus on the periodic domain Ω from the infinitely large reticle domain; i.e. $x \in (-\frac{L}{2}, \frac{L}{2})$ and $y \in (-\frac{h}{2}, \frac{h}{2})$. The internal potential energy is given by

$$U_{int} = \int_{\Omega} \frac{1}{2}\sigma_{ij}\epsilon_{ij}\,. \tag{2.35}$$

The contribution of external loads is

$$U_{ext} = -\int_{\partial\Omega} \mathbf{t}\cdot\mathbf{u}\,, \tag{2.36}$$

where $\mathbf{t}$ is the traction vector given by $\mathbf{t} = -\sigma_{yy}\mathbf{e_y}$ at $y = -\frac{h}{2}$ and $\mathbf{t} = \mathbf{0}$ at $y = \frac{h}{2}$. At $x = \pm L/2$ there is no contribution since there is only a normal traction on surfaces with normal $\mathbf{n} = \pm\mathbf{e_x}$ and the displacement u_x equals zero. The potential energy in this domain is then

$$U_{pot} = U_{int} + U_{ext}\,. \tag{2.37}$$

Due to periodicity, it can be shown that minimizing the overall (infinitely large) potential energy is equivalent to minimizing this partial potential energy of this domain. Thus, to find the parameters C_i, one needs to solve the linear equation system

$$\frac{\partial}{\partial C_i} U_{pot} = 0\,, \tag{2.38}$$

for $i = (1, 2, .., 8)$. As expected, the resulting $\mathbf{u}$, c_T and σ match the exact solution as derived in the previous section.

2.3 Edge Effects: Bounded x-Domain

In this section we want to deal with the case where the reticle has finite dimension in the x-direction. This can be illustrated by looking at Figure 3 and imagine the dashed lines at $x = \pm L/2$ as solid boundary of the reticle geometry.

Let us consider the same loading at $y = \pm L/2$ as in the previous section. As we can see in Equation (2.8) and (2.10), σ_{xy} vanishes at $x = \pm L/2$ whereas $\sigma_{xx}(x = \pm L/2) \neq 0$. This normal stress is related to bending of the reticle. In real e-chucking there is a traction free surface at $x = \pm L/2$. To get the solution to this boundary condition one can assume in a first step the boundary conditions at $x = \pm L/2$ to be given as

$$\begin{aligned}
\sigma_{xx}(L/2, y) &= A(-1)^n \{\cosh(\alpha y)\,[K_1 + yK_3] \\
&\qquad - \sinh(\alpha y)\,[K_2 + yK_4]\} && (2.39)\\
\sigma_{xy}(L/2, y) &= 0 && (2.40)\\
\sigma_{xx}(-L/2, y) &= A(-1)^n \{\cosh(\alpha y)\,[K_1 + yK_3] \\
&\qquad - \sinh(\alpha y)\,[K_2 + yK_4]\} && (2.41)\\
\sigma_{xy}(-L/2, y) &= 0 && (2.42)\\
\sigma_{yy}(x, h/2) &= 0 && (2.43)\\
\sigma_{yx}(x, h/2) &= 0 && (2.44)\\
\sigma_{yy}(x, -h/2) &= A\cos(\alpha x) && (2.45)\\
\sigma_{yx}(x, -h/2) &= 0\,, && (2.46)
\end{aligned}$$

where $n = 1, 2, \ldots$ and we made use of Equation (2.8). This gives the same solution for the displacement field $\mathbf{u}$ in the bounded x-domain as in the previous section.

In a second step one needs to find the solution to the following boundary conditions:

$$\begin{aligned}\sigma_{xx}(L/2,y) &= A(-1)^{n-1}\{\cosh(\alpha y)\,[K_1+yK_3] \\ &\quad -\sinh(\alpha y)\,[K_2+yK_4]\} \qquad (2.47)\\ \sigma_{xy}(L/2,y) &= 0 \qquad (2.48)\\ \sigma_{xx}(-L/2,y) &= A(-1)^{n-1}\{\cosh(\alpha y)\,[K_1+yK_3] \\ &\quad -\sinh(\alpha y)\,[K_2+yK_4]\} \qquad (2.49)\\ \sigma_{xy}(-L/2,y) &= 0 \qquad (2.50)\\ \sigma_{yy}(x,h/2) &= 0 \qquad (2.51)\\ \sigma_{yx}(x,h/2) &= 0 \qquad (2.52)\\ \sigma_{yy}(x,-h/2) &= 0 \qquad (2.53)\\ \sigma_{yx}(x,-h/2) &= 0\,. \qquad (2.54)\end{aligned}$$

The resulting displacement field is called $\mathbf{w}$ in this context. It can be estimated by modeling the boundary conditions as:

$$\tilde{\sigma}_{xx}(\pm L/2,y) = k_1\cdot y + k_2\,, \qquad (2.55)$$

such that the statically equivalent normal force and bending moment remain the same; i.e. demanding

$$\begin{aligned}\int_{-h/2}^{h/2}\sigma_{xx}(L/2,y)dy &= \int_{-h/2}^{h/2}\tilde{\sigma}_{xx}(L/2,y)dy = k_2\cdot h\,, \qquad (2.56)\\ \int_{-h/2}^{h/2} y\cdot\sigma_{xx}(L/2,y)dy &= \int_{-h/2}^{h/2} y\cdot\tilde{\sigma}_{xx}(L/2,y)dy = \frac{k_1h^3}{12}\,. \qquad (2.57)\end{aligned}$$

Solving this gives us

$$\begin{aligned}k_1 &= \frac{12A}{\alpha^2h^3}\cos(\frac{\alpha L}{2}) = \frac{3AL^2}{\pi^2n^2h^3}(-1)^n =: k\,, \qquad (2.58)\\ k_2 &= 0\,. \qquad (2.59)\end{aligned}$$

Then we know from linear, isotropic elasticity that

$$\begin{aligned}w_{x,x} &= \epsilon_{xx} = \frac{1}{\bar{E}}\tilde{\sigma}_{xx} = \frac{1}{\bar{E}}ky\,, \qquad (2.60)\\ w_{y,y} &= \epsilon_{yy} = -\frac{\bar{\nu}}{\bar{E}}\tilde{\sigma}_{xx} = -\frac{\bar{\nu}}{\bar{E}}ky\,. \qquad (2.61)\end{aligned}$$

Upon integration and demanding that the reticle is fixed at the origin and no rotation occurs we get

$$\begin{aligned}w_x &= \frac{k}{\bar{E}}xy \qquad (2.62)\\ w_y &= -\frac{k\bar{\nu}}{2\bar{E}}y^2 - \frac{k}{2\bar{E}}x^2\,. \qquad (2.63)\end{aligned}$$

Applying the superposition principle, **u** and **w** give the solution

$$u_{x,tot} = u_x + w_x \tag{2.64}$$
$$u_{y,tot} = u_y + w_y \tag{2.65}$$

to the mechanical boundary value problem on a finite domain with boundary conditions

$$\begin{aligned}
\sigma_{xx}(L/2, y) &= 0 && (2.66)\\
\sigma_{xy}(L/2, y) &= 0 && (2.67)\\
\sigma_{xx}(-L/2, y) &= 0 && (2.68)\\
\sigma_{xy}(-L/2, y) &= 0 && (2.69)\\
\sigma_{yy}(x, h/2) &= 0 && (2.70)\\
\sigma_{yx}(x, h/2) &= 0 && (2.71)\\
\sigma_{yy}(x, -h/2) &= A\cos(\alpha x) && (2.72)\\
\sigma_{yx}(x, -h/2) &= 0\,. && (2.73)
\end{aligned}$$

It has been observed that the influence of **w** is not negligible. To illustrate this we define

$$w_{bs} := |w_y(x = L/2, y = -h/2)|\,. \tag{2.74}$$

Let us assume the numerical values $\nu = 0.17$, $E = 67.6$ GPa, which correspond to plane-strain-moduli $\bar{\nu} = 0.2$ and $\bar{E} = 69.6$ GPa, a pressure amplitude of $A = 15$ kPa and geometric properties $h = 6.35$ mm, $L = 152$ mm. The resulting displacement amplitudes u_{bs} and u_{fs} for the unbounded x-domain solution can be seen in Figure 5 (see also Section 3.2 for a more detailed discussion). The influence of edge effects is determined by the magnitude of w_{bs}. In Figure 5 a clear dominance of w_{bs} can be observed.

2.4 How to Deal with Cosine Warped Surfaces in a Bounded x-Domain

As we have seen in the last section, applying a cosine-pressure-profile on the backside surface does not result in a cosine warped backsurface when the x-domain is bounded. The aim is however to predict the transmission of cosine-like features, which would allow for using Fourier or Cosine transformations to deal with regular surface shapes. Hence we would need to search for appropriate stress boundary conditions on the backsurface which would result in a cosine-like u_y displacement on the backside. Knowing this solution we would then be able to predict the result on the frontside. Or, vice versa, one needs to find a solution of the mixed boundary value problem related to displacements at the backside and stress free boundaries elsewhere.

Finding an analytical solution to this problem is however not trivial and the question is whether there exists a solution at all (think of uniqueness of solutions and the fact that only

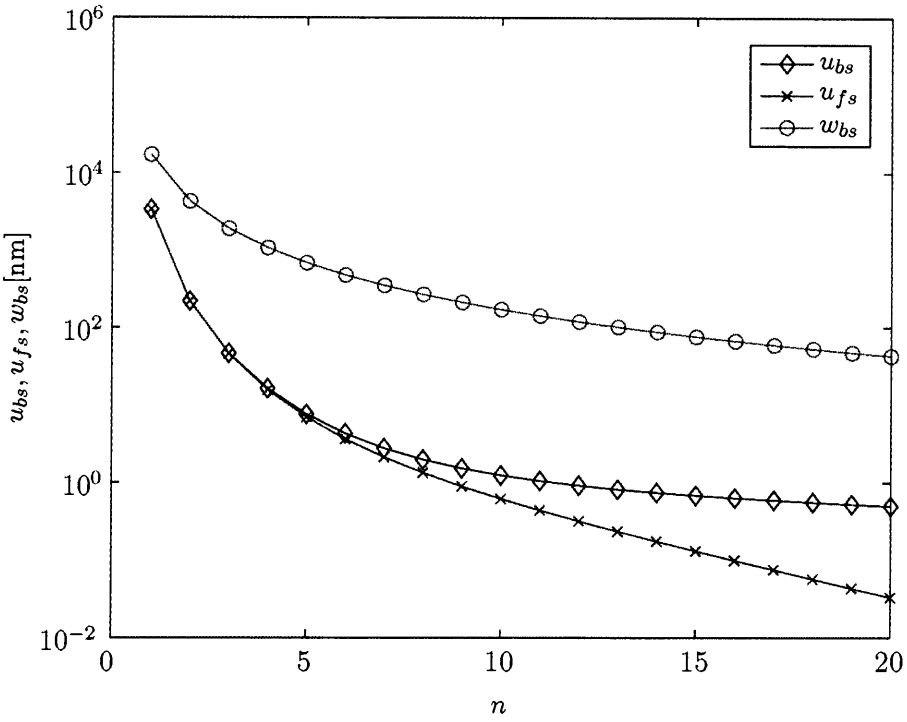

Figure 5: Displacement contributions at ideal flattening with $A = 15$ kPa. Amplitudes u_{bs} and u_{fs} of the solution in an unbounded x-domain. Influence of edge effects in a bounded x-domain (w_{bs}).

a non-zero stress boundary condition at boundary edges $x = \pm L/2$ resulted in a cosine like displacement on the reticle backside). Finite element simulations, however, have shown, that at real e-chucking of a cosine warped reticle backside also a cosine-like feature is transmitted to the frontside. This is especially true for higher wavenumbers. Hence, in the following analytical considerations of the transmitted amplitude, we will only take the solution of an infinitely large reticle into account, keeping possible edge effects in mind.

3 Two Dimensional E-Chucking

We now take a closer look at the real e-chucking process. At first we regard the reticle as infinitely large in the x-direction. As ideal e-chucking we refer to an analytical solution in an unbounded x-domain and a special assumption on the contact forces acting on a cosine-warped backsurface when brought into contact with a flat chuck. We will see how a maximum value on removable backside non-flatness is imposed by the applied voltage on a bipolar chuck. The discrete cosine transformation allows us to define an algorithm, which makes use of the derived theoretical results and predicts the reticle frontside shape after ideal e-chucking. We illustrate this method with a numerical example of a randomly chosen spline surface. Later in this chapter we perform a finite element calculation of a more realistic chuck-reticle model with finite x-dimensions and compare both results.

3.1 Ideal, Complete E-Chucking

The model of ideal, complete e-chucking is illustrated in Figure 6. A cosine warped backsurface is brought into contact with a rigid flat chuck surface. In the case of an infinitely large reticle one can assume that such a surface could be flattened out completely. The question is then, what forces are acting on the boundary, which would us allow to define a connection to the solution of the ideal flattening model.

The pressure on the reticle backside results from an electrostatic field. When applying the voltage U on a bipolar e-chuck, the pressure acting on the conducting reticle's backside respectively the chuck's electrodes can be approximated by

$$p = \frac{\epsilon_0 \epsilon^2 U^2}{8(\epsilon \delta_a + \delta_d)^2}, \tag{3.1}$$

where $\epsilon_0 = 8.85\ \frac{\mathrm{A^2 s^4}}{\mathrm{kgm^3}}$ is the vacuum permittivity, ϵ the relative dielectric constant of the chuck, δ_d the thickness of the dielectric and δ_a the air gap. For numerical illustration we will assume later $\epsilon = 8$ and $\delta_d = 150\ \mu$m. Let us assume the state where complete chucking occurs but a small reduction in the voltage would result in a non-complete chucking state. This would mean that the air gap $\delta_a = 0$ and hence

$$p_{chuck} = \frac{\epsilon_0 \epsilon^2 U^2}{8\delta_d^2}. \tag{3.2}$$

In order to get the overall pressure acting on the reticle backsurface one needs to take the contact forces into account. Motivated by the solution of the Hertz contact problem and due to small deformations, one can assume that

$$p_{contact} = -p_{chuck} \cdot (1 - \cos(\alpha x)). \tag{3.3}$$

The overall normal stress on the reticle backside surface is thus

$$\sigma_{yy,real} = p_{chuck} + p_{contact} = p_{chuck} \cdot \cos(\alpha x). \tag{3.4}$$

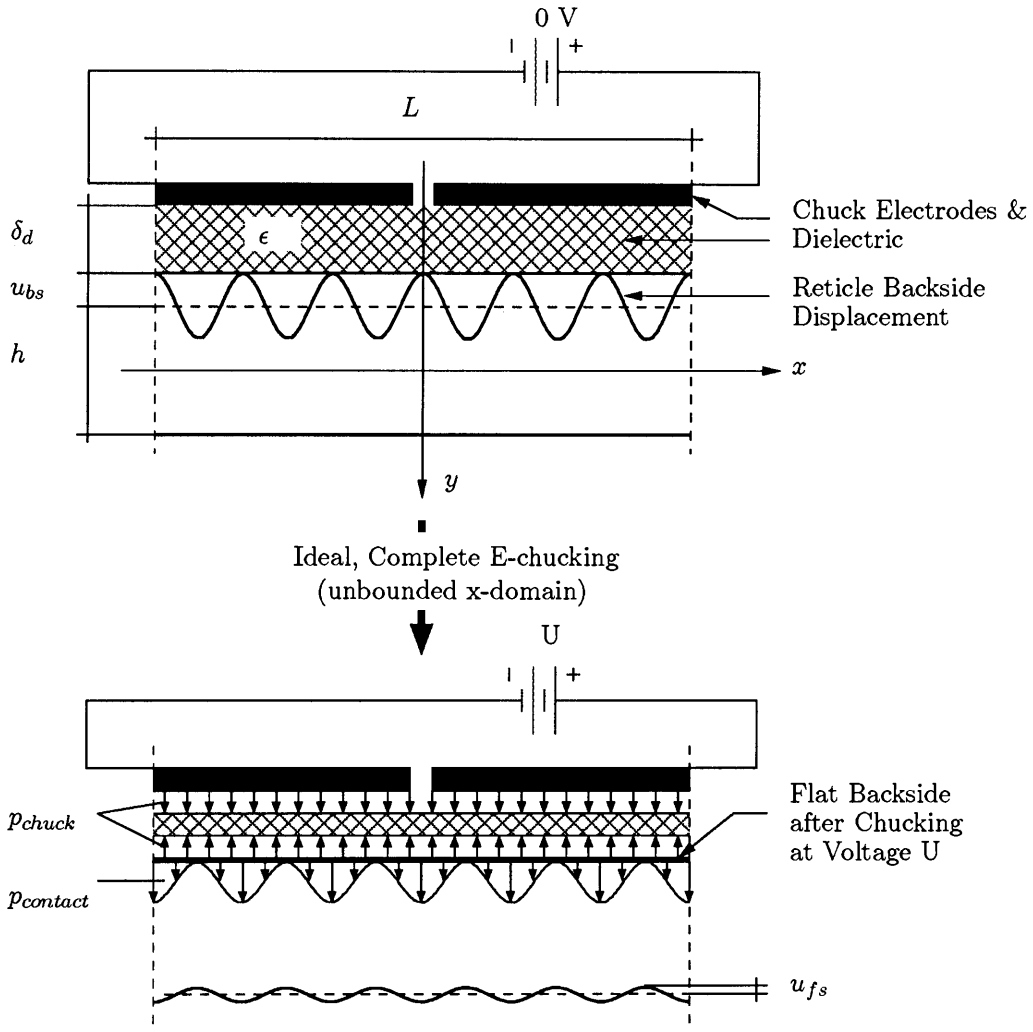

Figure 6: Two dimensional idealization of reticle geometry before and after ideal, complete e-chucking.

A comparison with Equation (2.3) gives

$$A = p_{chuck} = \frac{\epsilon_0 \epsilon^2 U^2}{8\delta_d^2}, \tag{3.5}$$

the connection between ideal flattening with pressure magnitude A and ideal e-chucking at voltage U.

3.2 Maximum Allowable Backside Amplitude

Knowing this pressure-to-voltage connection allows us to ask for the maximum allowable amplitude for a given wavelength, that could be flattened when applying a voltage U. Let us first return to the ideal flattening case. By evaluating Equation (2.25) at $y = -h/2$ the amplitude of the backside displacement for a given pressure amplitude A is given by

$$u_{bs} = \frac{2A \cdot (1-\bar{\nu}^2) \cdot (2\alpha h + \sinh(2\alpha h))}{\alpha \cdot \bar{E} \cdot (1 + 2(\alpha h)^2 - \cosh(2\alpha h))}. \tag{3.6}$$

As observed for the transmission coefficient, there is a dependancy on the wavenumber n and the dimensionless parameter d. In addition the Poisson ratio ν, the E-modulus of the reticle as well as the reticle length L do influence the amplitude. To give a numerical example we set $\nu = 0.17$, $E = 67.6$ GPa, which corresponds to plane-strain-moduli $\bar{\nu} = 0.2$ and $\bar{E} = 69.6$ GPa. Let us assume a pressure amplitude of $A = 15$ kPa. The resulting displacement amplitude u_{bs} for varying d and L is plotted in Figure 7 and Figure 8. In both plots the general trend is observed that at a fixed pressure/voltage higher backside amplitudes occur for lower wavenumbers.

At ideal e-chucking the maximum allowable backside amplitude $\bar{u}_{bs,2d}$ which is transferred to the frontside, depending on the applied voltage and chuck properties, can be computed by the use of Equation (3.6) and (3.5):

$$\bar{u}_{bs,2d} = \frac{\epsilon_0 \epsilon^2 U^2 \cdot (1-\bar{\nu}^2) \cdot (2\alpha h + \sinh(2\alpha h))}{4\delta_d^2 \cdot \alpha \cdot \bar{E} \cdot (1 + 2(\alpha h)^2 - \cosh(2\alpha h))}. \tag{3.7}$$

The result for $\epsilon = 8$, $\delta_d = 150$ μm and $U = 1000, 2000, 3000$ V is shown in Figure 9.

3.3 Ideal, Non-Complete E-chucking in 2D

In order to compute the transmitted frontside amplitude u_{fs} one can assume that when u_{bs} exceeds $\bar{u}_{bs,2d}$ only the fraction $\bar{u}_{bs,2d}$ is transmitted to the frontside. Therefore we propose:

$$u_{fs} = c_{T,2d} \cdot min(u_{bs}, \bar{u}_{bs,2d}) \tag{3.8}$$

as an analytical estimate of the resulting frontside non-smoothness due to backside cosine perturbations. A verification of this estimate is given in the end of Section 3.5.

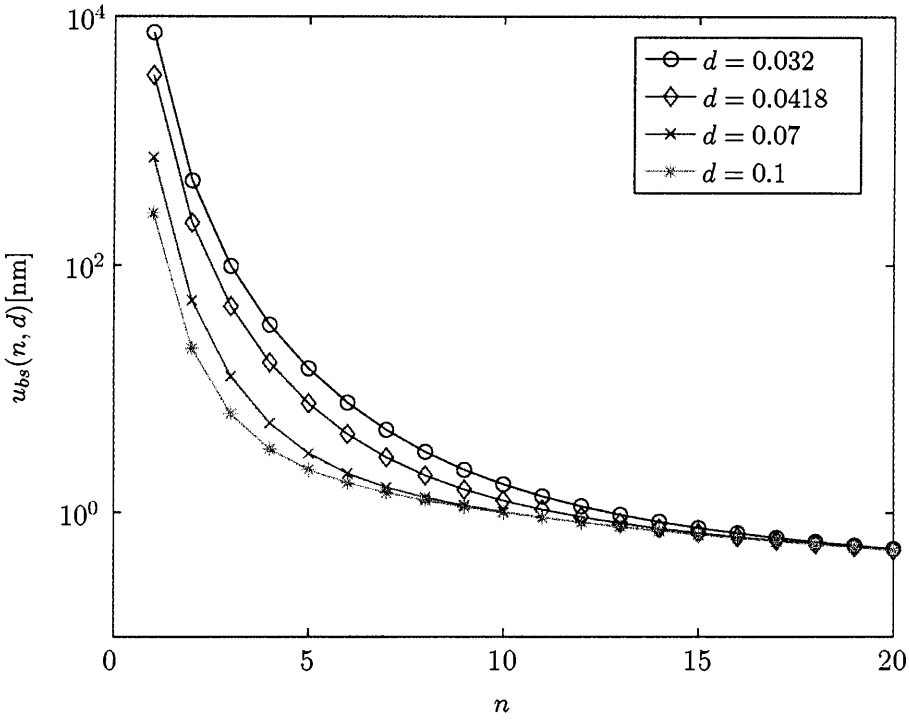

Figure 7: Amplitude of backside displacement for varying d ($A = 15$ kPa, $L = 152$ mm).

3.4 General Surface Shapes, One Dimensional DCT

Next we wish to develop a method to compute the transmission of a general reticle backside surface shape.

The discrete cosine transform X of a vector x is given by

$$X_k = \frac{2}{N}\sum_{i=0}^{N-1} x_i \cdot \cos(\frac{\pi}{N}(i+\frac{1}{2})k)\,,\ k = 0, 1, \ldots, N-1\,, \tag{3.9}$$

where N is the length of the vector x. The inverse cosine transform is then given by

$$x_i = \frac{1}{2}X_0 + \sum_{k=1}^{N-1} X_k \cdot \cos(\frac{\pi}{N}(i+\frac{1}{2})k)\,,\ i = 0, 1, \ldots, N-1. \tag{3.10}$$

The scaling has been chosen such that $|X_k|$ measures the amplitude of the corresponding wave for $k \neq 0$ and $|X_0|/2$ the mean value. Odd $k = 1, 3, 5, \ldots$ relate to $\sin(\frac{k\cdot\pi}{L}x)$-waves and $k = 2, 4, 6, \ldots$ relate to $\cos(\frac{k\cdot\pi}{L}x)$-waves in the surface shape in our coordinate system; i.e. $k = 2, 4, 6, \ldots$ correspond to wavenumbers $n = 1, 2, 3, \ldots$ according to the previous section. If one has an even-symmetrical shape around the origin, one can just replace $k \to 2k$ in

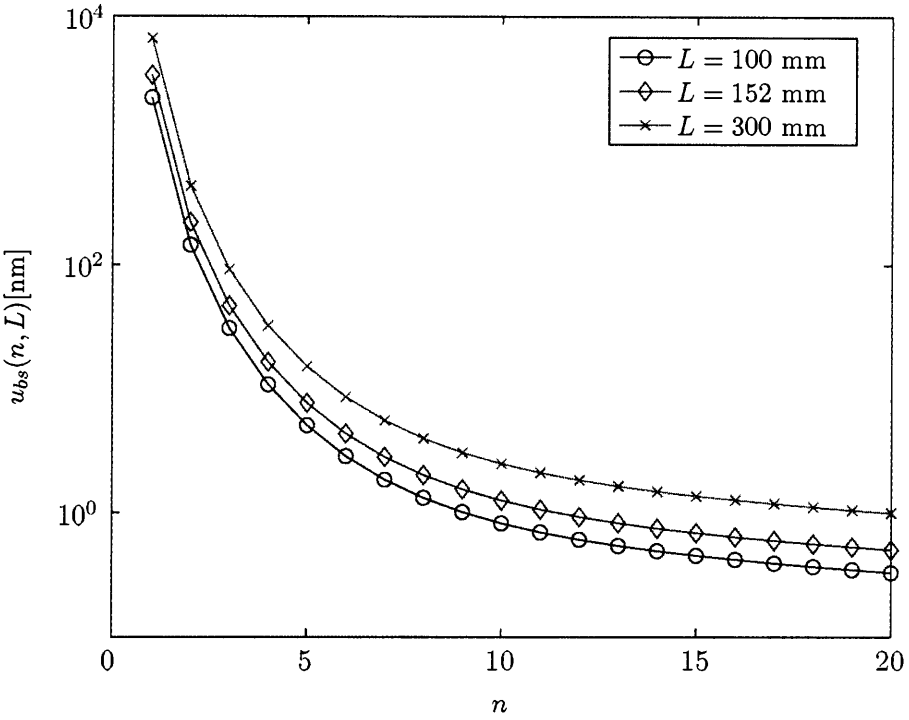

Figure 8: Amplitude of backside displacement for varying L ($A = 15$ kPa, $d = 0.0418$).

Equation (3.9) and (3.10). This means choosing as basis functions only $\cos(\frac{2n\cdot\pi}{L}x)$-waves. Then one can directly apply Equation (3.8), where $u_{bs}(n)$ would correspond to $|X(k)|$, and the inverse transformation of $u_{fs}(n)$ would give the frontside surface shape after chucking.

In order to handle non-even-symmetrical surface shapes we also allow for basis functions with $k = 1, 3, 5, \ldots$. In the analytical description so far they have been omitted since we only considered a self-equilibrated pressure profile with zero resulting moment. In the real e-chucking case these moments would need to be compensated for by (edge) contact forces.

In the following we denote as y_{bs} the general backside perturbation before chucking and y_{fs} the frontside displacement after chucking. The spectral counterparts are defined as Y_{bs} and Y_{fs}. To compute the frontside surface shape y_{fs} after chucking one needs to apply the following procedure:

- Given data vector y_{bs}: compute discrete cosine transform $Y_{bs}(k)$ according to Equation (3.9).

- Given voltage U: compute allowable backside amplitude $\bar{u}_{bs,2d}(n)$ according to Equation (3.7).

- Set $Y_a = Y_{bs}$. For $k = 1, 2, .., N-1$ check wether $|Y_a(k)|$ exceeds $\bar{u}_{bs,2d}(n = k/2)$. If

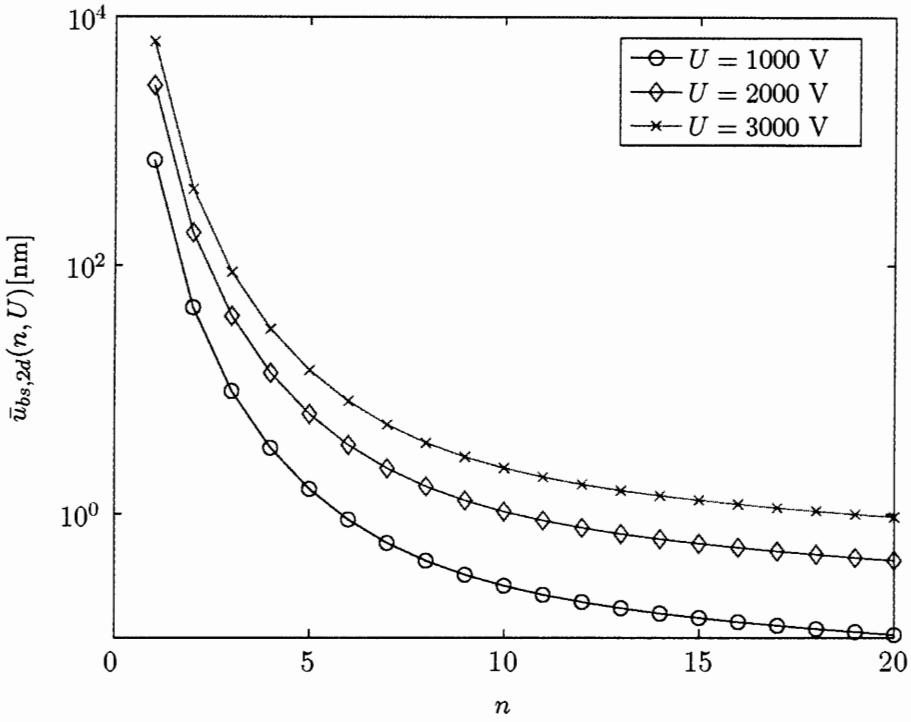

Figure 9: Maximum allowed backside amplitude for complete ideal e-chucking of a bipolar chuck-reticle system.

yes, set

$$Y_a(k) = sign(Y_a(k)) \cdot \bar{u}_{bs,2d}(n = k/2)\,. \tag{3.11}$$

- Set $Y_{fs} = Y_a$. For $k = 1, 2, \ldots, N-1$ compute

$$Y_{fs}(k) = c_{T,2d}(n = k/2) \cdot Y_{fs}(k)\,, \tag{3.12}$$

$c_{T,2d}$ according to Equation (2.28).

- Compute the inverse discrete cosine transform y_{fs} of Y_{fs} according to Equation (3.10).

- To get the final frontside surface shape set $y_{fs} = -y_{fs}$.

To illustrate this we show an example in Figures 11 and 12. In the spectral decomposition one can see how the maximum allowed amplitude $\bar{u}_{bs,2d}$ cuts off the high frequencies at $U = 2000$ V. Increasing the voltage would allow for smaller wavelengths to be chucked. However, the transmission coefficient $c_{T,2d}$ would then damp these higher wavenumbers.

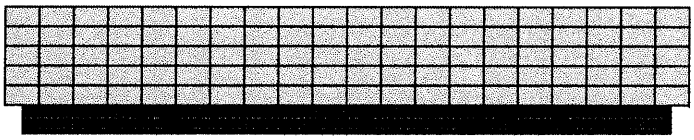

Figure 10: Finite element mesh of reticle (bottom) and chuck (top) for two dimensional analysis of real e-chucking.

3.5 FEA of 2D Real E-Chucking

To verify the analytical solution of the overall transmission in two dimensions for a fixed voltage U we perform a finite element calculation with FEAP of a chuck-reticle two-body contact problem. The properties of such an analysis in three dimensions are discussed in Section 4.4. In order to do this analysis for a plane strain case in two dimensions, we have used basically the same model as for the three dimensional case with slight modification of the chuck and reticle mesh as well as the boundary condition.

The chuck mesh is changed to a simple Cartesian block with $20 \times 1 \times 5$ equi-sized 8-node hexahedral elements and overall dimension $160 \times 1 \times 22.6$ mm. The reticle mesh is changed to a Cartesian block with $100 \times 1 \times 8$ equi-sized 8-node hexahedral elements and overall dimension $152 \times 0.1 \times 6.35$ mm (see Figure 10). The warping of the reticle backside is done in analogy to the three dimensional case and can be seen on top of Figure 11. In order to obtain a plane strain simulation, the displacement boundary conditions on the reticle in the third dimension are set to zero.

The result of the displacement y_{feap} when applying a voltage $U = 2000$ V can be seen at the bottom of Figure 11. The spectral components Y_{feap} are also plotted in Figure 12.

In the spectral perspective we see that the high frequency components of Y_{feap} as well as Y_{fs} are below the estimate of $\bar{u}_{bs,2d}$. If we had only taken the transmission coefficient into account, the components of Y_{fs} would have been too large in comparison to the FEA result. This justifies the concept of the maximum allowable amplitude $\bar{u}_{bs,2d}$ and the assumption made in Equation (3.8).

3.6 Discussion

In order to predict the reticle frontside shape at a certain chucking voltage U, an analytical as well as a finite element calculation model have been developed. For illustration we took as input the spline surface as on top of Figure 11 and assumed a chucking voltage $U = 2000$ V. The result of the analytical calculation y_{fs} is plotted as solid line at the bottom of Figure 11 and the result of the finite element calculation is shown as dashed line. The spectral components of the input data before chucking Y_{bs}, of the analytical prediction Y_{fs}, as well as of the FEAP calculation are shown in Figure 12.

It can be seen that for each method high spatial frequencies ($k > 6$) are clearly damped out. This means that backside features with wavenumber greater than $n = 3$ are not expected to be observed at the chucked frontside. The cut-off is in good accordance with the theoretical

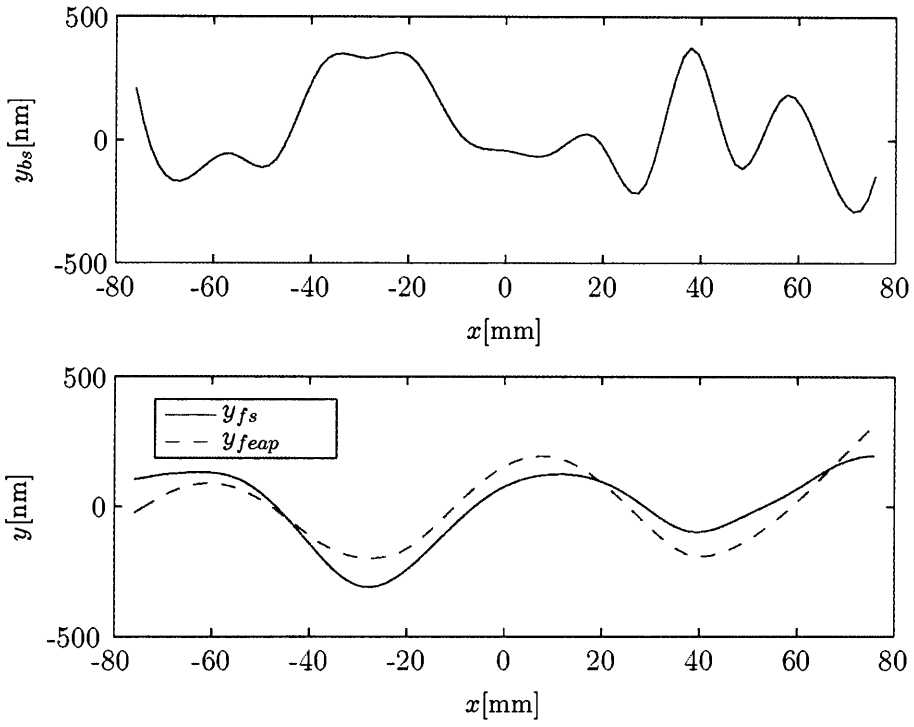

Figure 11: Example of two dimensional feature transfer, out-of-plane-distortion. Top: Reticle backsurface shape y_{bs} before e-chucking. Bottom: frontside shape y_{fs} according to analytical prediction of ideal e-chucking at voltage $U = 2000$ V and FEAP simulation output y_{feap} of real e-chucking at voltage $U = 2000$ V.

prediction of a maximum allowable amplitude $\bar{u}_{bs}$, which is also plotted in Figure 12.

For wavenumbers smaller or equal $n = 3$, i.e. $k \leq 6$, there occurs a deviation between analytical prediction and finite element calculation, even if the overall shapes match pretty well.

It is important to note that the analytical calculation is based on the assumption that the reticle is unbounded in x-direction, whereas the finite element analysis has a bounded x- and y-domain. This might explain the deviation in the two solutions (see Section 2.4).

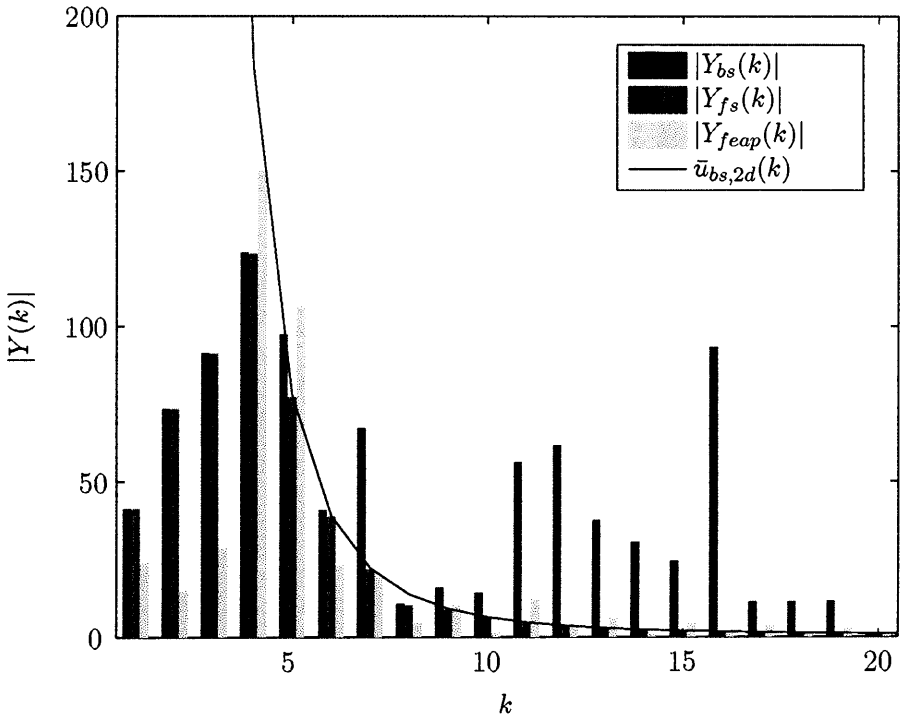

Figure 12: Example of two dimensional feature transfer, spectral perspective. Spectral components of reticle backside pertubation Y_{bs} before e-chucking, spectral components of frontside shape Y_{fs} according to analytical prediction of ideal e-chucking at voltage $U = 2000$ V, discrete cosine transform of FEAP simulation output of real e-chucking Y_{feap} at voltage $U = 2000$ V, maximum allowable amplitude prediction $\bar{u}_{bs,2d}(k)$ at $U = 2000$ V.

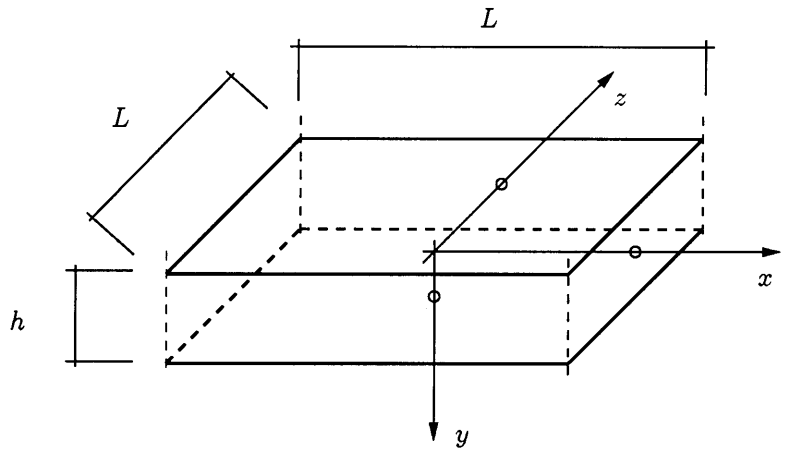

Figure 13: Reticle geometry in three dimensions. Unbounded x,z-domain and centered coordinate system.

4 Three Dimensional Case

In this section we extend the main ideas of the last two sections to the three dimensional case. At first we derive the transmission coefficient in three dimensions via an approximation, flollowing the two dimensional ideal flattening case with an unbounded x-domain. As an output of this calculation we also obtain the maximum allowable amplitude for the ideal e-chucking case. As was done in the two dimensional case, we will define an algorithm using discrete cosine transformations to predict the transmission of an arbitrary backside surface shape to the frontside during ideal e-chucking. An example is shown and compared to a finite element calculation.

4.1 Transmission Coefficient in 3D

In this section we want to derive the transmission coefficient for the three dimensional case. Let us consider the geometry as plotted in Figure 13. We regard the reticle as infinitely large in x, z-direction. It is difficult to derive a closed form analytical solution for the mechanical boundary value problem as was done in the two dimensional case. Therefore we make a guess on the function-space for the displacement field and minimize the resulting potential energy to find the proper coefficients.

Using this method one first needs to define a basis for the displacement field. In the two dimensional case it has been observed that choosing the ansatz functions

$$u_y = \cos(\alpha x) \cdot (C_1 \cosh(\alpha y) + C_2 \sinh(\alpha y) + C_3 y \cosh(\alpha y) + C_4 y \sinh(\alpha y)) \tag{4.1}$$

$$u_x = \sin(\alpha x) \cdot (C_5 \cosh(\alpha y) + C_6 \sinh(\alpha y) + C_7 y \cosh(\alpha y) + C_8 y \sinh(\alpha y)) \tag{4.2}$$

according to Equations (2.29), (2.30) results in the exact solution when minimizing the resulting potential energy for the free parameters C_i. The x-dependancy of the analytical solution of u_x, u_y is in accordance to the applied external load on the reticle backside. The y-dependancy is in accordance to assuming an Airy stress function and requiring the bi-harmonic equation $\nabla^4\Phi = 0$ to be satisfied.

For the three dimensional case we choose the following external load on the reticle's backside:

$$\sigma_{yy}(x, -h/2, z) = A\cos(\alpha x)\cos(\alpha z)\,. \tag{4.3}$$

By analogy as in two dimensions we propose that

$$\begin{aligned} u_y &= \cos(\alpha x)\cos(\alpha z) f_y(y) && (4.4)\\ u_x &= \sin(\alpha x)\cos(\alpha z) f_x(y) && (4.5)\\ u_z &= \cos(\alpha x)\sin(\alpha z) f_z(y)\,. && (4.6) \end{aligned}$$

Motivated by [1] we assume the existence of a potential Φ such that the compatibility equations for the mechanical boundary value problem read

$$\nabla^6\Phi = 0\,; \tag{4.7}$$

i.e., satisfying let's say a tri-harmonic equation. In analogy to the two dimensional case we assume

$$\Phi(x, y, z) = \cos(\alpha x)\cos(\alpha z) f(y). \tag{4.8}$$

Solving Equations (4.7) and (4.8) without any boundary conditions results in

$$f(y) \in \operatorname{span}\{f_1, f_2, f_3, f_4, f_5, f_6\}\,, \tag{4.9}$$

where

$$\begin{aligned} f_1 &= \cosh(\sqrt{2}\alpha y) && (4.10)\\ f_2 &= \sinh(\sqrt{2}\alpha y) && (4.11)\\ f_3 &= y\cosh(\sqrt{2}\alpha y) && (4.12)\\ f_4 &= y\sinh(\sqrt{2}\alpha y) && (4.13)\\ f_5 &= y^2\cosh(\sqrt{2}\alpha y) && (4.14)\\ f_6 &= y^2\sinh(\sqrt{2}\alpha y)\,. && (4.15) \end{aligned}$$

Hence we choose the following ansatz function for the displacement field:

$$\begin{aligned} u_y &= \cos(\alpha x)\cos(\alpha z)(C_1 f_1 + C_2 f_2 + C_3 f_3 + C_4 f_4 + C_5 f_5 + C_6 f_6) && (4.16)\\ u_x &= \sin(\alpha x)\cos(\alpha z)(C_7 f_1 + C_8 f_2 + C_9 f_3 + C_{10} f_4 + C_{11} f_5 + C_{12} f_6) && (4.17)\\ u_z &= \cos(\alpha x)\sin(\alpha z)(C_{13} f_1 + C_{14} f_2 + C_{15} f_3 + C_{16} f_4 + C_{17} f_5 + C_{18} f_6). && (4.18) \end{aligned}$$

Having chosen a displacement field we can proceed as for the two dimensional case discussed in Section 2.2. Assuming linear elasticity the strain tensor field ϵ is computed by

$$\epsilon_{ij} = \frac{1}{2}(u_{i,j} + u_{j,i}) , \tag{4.19}$$

where $i, j \in (x, y, z)$. The Lame-parameters are given by

$$\mu = \frac{E}{2(1+\nu)} \tag{4.20}$$

$$\lambda = \frac{\nu E}{(1-2\nu)(1+\nu)} . \tag{4.21}$$

Then the stress field σ can be computed by

$$\sigma_{ij} = 2\mu\epsilon_{ij} + \lambda\delta_{ij}\epsilon_{kk} . \tag{4.22}$$

Let us again focus on the periodic domain Ω from an infinitely large reticle domain; i.e. $x, z \in (-\frac{L}{2}, \frac{L}{2})$ and $y \in (-\frac{h}{2}, \frac{h}{2})$. The internal potential energy is given by

$$U_{int} = \int_{\Omega} \frac{1}{2}\sigma_{ij}\epsilon_{ij} . \tag{4.23}$$

The contribution of external loads is

$$U_{ext} = -\int_{\partial\Omega} \mathbf{t} \cdot \mathbf{u} , \tag{4.24}$$

where $\mathbf{t}$ is the traction vector given by $\mathbf{t} = -\sigma_{yy}\mathbf{e_y}$ at $y = -\frac{h}{2}$ and $\mathbf{t} = \mathbf{0}$ at $y = \frac{h}{2}$. There is no contribution on $x, z = \pm L/2$ since there is only a normal traction on surfaces with normal $\mathbf{n} = \pm\mathbf{e_x}, \mathbf{e_z}$ and the displacements u_x, u_z equal zero.

The potential energy in this domain is then

$$U_{pot} = U_{int} + U_{ext} . \tag{4.25}$$

To find the parameters C_i one needs to solve the linear equation system

$$\frac{\partial}{\partial C_i} U_{pot} = 0 , \tag{4.26}$$

for $i = (1, 2, \ldots, 18)$.

In order to validate the correctness of this approximation we can monitor the stress components at the boundary. They match exactly the assumed boundary conditions on the surfaces $y = \pm h/2$. Namely, the normal stress $\sigma_{yy}(x, -h/2, z) = A\cos(\alpha x)\cos(\alpha z)$ and $\sigma_{yy}(x, h/2, z) = 0$. At the areas $x, z = \pm L/2$ we observe a zero shear stress component and a linear dependancy of the normal stress on y with a zero mean average as observed in the

two dimensional case. This justifies, though does not prove, the correctness of assuming the potential function to satisfy Equation (4.7).

Knowing the parameters C_i, we can compute the transmission coefficient

$$c_{T,3d} = \frac{u_y(x, y = h/2, z)}{u_y(x, y = -h/2, z)} . \tag{4.27}$$

Since it was not possible to get a nice printable symbolic solution we give here only numerical results for $n = 1, 2, \ldots, 20$ choosing $h = 6.35$ mm, $L = 152$ mm which are plotted in Figure 14. As expected, no dependancy on E, ν and A is observed.

To be able to implement a frequency filter via the discrete cosine transform as for the two dimensional case, one needs to define an analytical approximation to the numerical results. The two dimensional analytical result for the same geometric properties, i.e. $d = 0.0418$, is plotted in Figure 14. A fitting of the three dimensional values can be obtained easily by calling the function $c_{T,2d}$ at a matching parameter d. In our example we find

$$c_{T,3d,fit}(d = 0.0418) = c_{T,2d}(d = 0.059) . \tag{4.28}$$

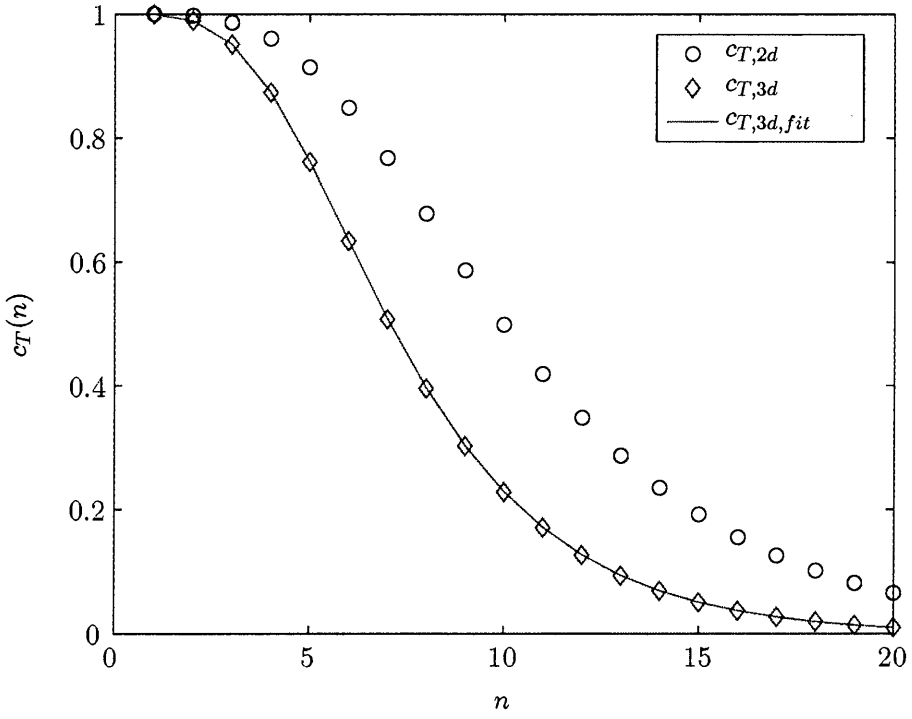

Figure 14: Transmission coefficient in two and three dimensions for $d = 0.418$.

4.2 Maximum Allowable Amplitude

The displacement amplitude on the backside is

$$u_{bs,3d} = |u_y(x, y = -h/2, z)| . \tag{4.29}$$

It is dependant on n, h, L, E, ν and A. In the following we assume $h = 6.35$ mm, $L = 152$ mm, $E = 67.6$ GPa, $\nu = 0.17$. Varying only A shows a linear dependancy for each n. As in the two dimensional case, one can assume that the maximum allowable amplitude $\bar{u}_{bs,3d}$, i.e. the connection to ideal e-chucking at voltage U, is computed by the evaluation of $u_{bs,3d}$ at $A \sim U^2$ according to Equation (3.5). The numerical results that come out of the energy minimization method described in the previous section are plotted for varying $U = 1000, 2000, 3000$ V and $n = 1, \ldots, 20$ in Figure 15.

As for the transmission coefficient one needs to define an analytical function for these values to be able to implement the saturation due to maximum allowable amplitude. Plotting the ratio $\frac{\bar{u}_{bs,3d}}{\bar{u}_{bs,2d}}$ for varying U shows about the same exponential growth for low wavenumbers n, whereas a saturation for higher wavenumbers $n > 7$ in the range of 0.7 occurs. Therefore we propose the following fitting. Take data of $\frac{\bar{u}_{bs,3d}}{\bar{u}_{bs,2d}}$ at 2000V for n up to 7. Do the least-square fitting for β_1 and β_2 of the ansatz function

$$\frac{\bar{u}_{bs,3d}}{\bar{u}_{bs,2d}} = \beta_1 e^{\beta_2 \cdot n} . \tag{4.30}$$

Then define the fitted $\bar{u}_{bs,3d,fit}$ as

$$\bar{u}_{bs,3d,fit} = min(\beta_1 e^{\beta_2 \cdot n}, 0.7) \cdot \bar{u}_{bs,2d} . \tag{4.31}$$

The result of $\beta_1 = 0.2281$ and $\beta_2 = 0.1012$ is plotted in Figure 15.

4.3 General Surface Shapes, Two Dimensional DCT

In order to handle two dimensional surface shapes we need to define the 2D DCT first.

$$X_{k_1,k_2} = \frac{4}{N_1 N_2} C(k_1) C(k_2) \sum_{i=0}^{N_1-1} \sum_{j=0}^{N_2-1} x_{i,j} \cdot \cos(\frac{\pi}{N_1}(i + \frac{1}{2})k_1) \cos(\frac{\pi}{N_2}(j + \frac{1}{2})k_2) , \tag{4.32}$$

where $k_1 = 0, 1, \ldots, N_1 - 1, k_2 = 0, 1, \ldots, N_2 - 1$, and

$$C(k) = \begin{cases} 1/\sqrt{2}, & \text{if } k = 0 \\ 1, & \text{if } k = 1, 2, 3, \ldots \end{cases} \tag{4.33}$$

The inverse transformation is then given by

$$x_{i,j} = \sum_{k_1=0}^{N_1-1} \sum_{k_2=0}^{N_2-1} C(k_1) C(k_2) X_{k_1,k_2} \cdot \cos(\frac{\pi}{N_1}(i + \frac{1}{2})k_1) \cos(\frac{\pi}{N_2}(j + \frac{1}{2})k_2) , \tag{4.34}$$

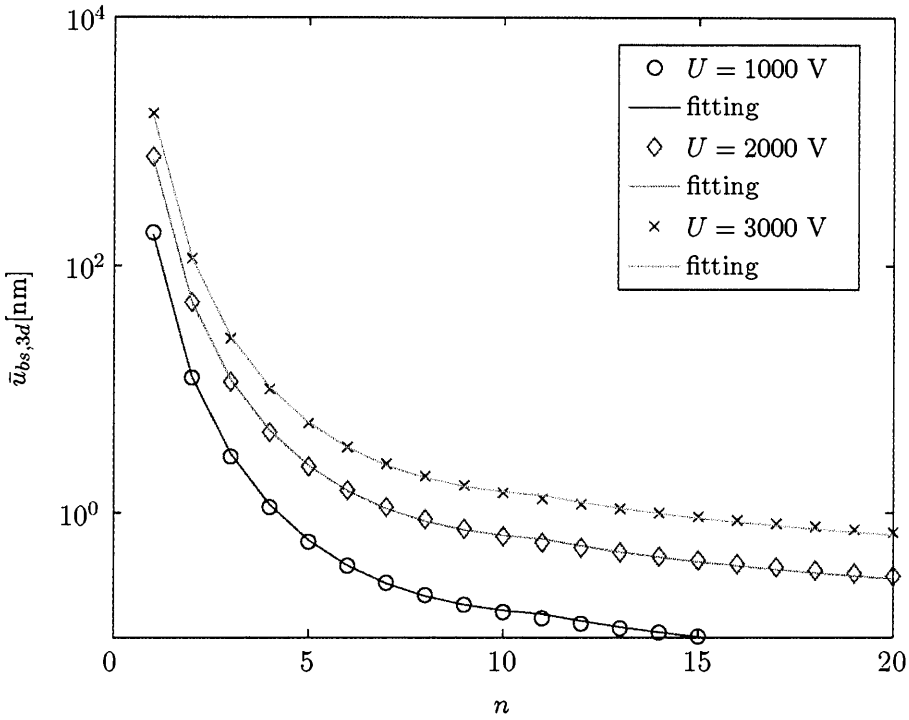

Figure 15: Maximum allowable amplitude in three dimensions. Analytical approximation and fitting method.

where $i = 0, 1, \ldots, N_1 - 1, j = 0, 1, \ldots, N_2 - 1$. The scaling has been chosen such that $|X_{k_1,k_2}|$ measures the amplitude of the corresponding basis function for $k_1 \neq k_2 \neq 0$, $|X_{0,0}|/2$ the mean value and $|X_{k_1,k_2}|/\sqrt{2}$ the amplitude if $k_1 = 0$ or $k_2 = 0$. In order to handle a general surface shape one needs to allow for $k_1 \neq k_2$. We assume that for the amount that is transmitted the maximum of k_1 and k_2 is important. Also, as for the two dimensional case, we allow for $k = 1, 3, 5, \ldots$ by calling $c_{T,3d,fit}(n = k/2)$ and $\bar{u}_{bs,3d,fit}(n = k/2)$. The mean value is not changed. For the cases $k_1 = 0$ or $k_2 = 0$ we take the functions $\bar{u}_{bs,2d}$ and $c_{T,2d}$ of the two dimensional solution. This leads to the following algorithm to compute the chucked frontside shape in three dimensions.

- Given data matrix $y_{bs}(i, j)$: compute discrete cosine transform $Y_{bs}(k_1, k_2)$ according to Equation (4.32).
- Given voltage U: compute allowable backside amplitude $\bar{u}_{bs,2d}(n)$ and $\bar{u}_{bs,3d,fit}(n)$ according to Equation (3.7) and (4.31).
- Set $Y_a = Y_{bs}$. For $k_1 = 0$, $k_2 = 1, 2, \ldots, N_2 - 1$ check whether $|Y_a(0, k_2)|/\sqrt{2}$ exceeds $\bar{u}_{bs,2d}(n = k_2/2)$. If yes, set

$$Y_a(0, k_2) = sign(Y_a(0, k_2)) \cdot \sqrt{2} \cdot \bar{u}_{bs,2d}(n = k_2/2)\,. \tag{4.35}$$

- For $k_2 = 0$, $k_1 = 1, 2, \ldots, N_1 - 1$ check whether $|Y_a(k_1, 0)|/\sqrt{2}$ exceeds $\bar{u}_{bs,2d}(n = k_1/2)$. If yes, set

$$Y_a(k_1, 0) = sign(Y_a(k_1, 0)) \cdot \sqrt{2} \cdot \bar{u}_{bs,2d}(n = k_1/2)\,. \tag{4.36}$$

- For $k_1 = 1, 2, \ldots, N_1 - 1$, $k_2 = 1, 2, \ldots, N_2 - 1$ check whether $|Y_a(k_1, k_2)|$ exceeds $\bar{u}_{bs,3d,fit}(n = max(k_1, k_2)/2)$. If yes, set

$$Y_a(k_1, k_2) = sign(Y_a(k_1, k_2)) \cdot \bar{u}_{bs,3d,fit}(n = max(k_1, k_2)/2)\,. \tag{4.37}$$

- Set $Y_{fs} = Y_a$. For $k_1 = 0$, $k_2 = 1, 2, \ldots, N_2 - 1$ compute

$$Y_{fs}(0, k_2) = c_{T,2d}(n = k_2/2) \cdot Y_{fs}(0, k_2)\,, \tag{4.38}$$

with $c_{T,2d}$ according to Equation (2.28).

- For $k_2 = 0$, $k_1 = 1, 2, \ldots, N_1 - 1$ compute

$$Y_{fs}(k_1, 0) = c_{T,2d}(n = k_1/2) \cdot Y_{fs}(k_1, 0)\,. \tag{4.39}$$

- For $k_1 = 1, 2, \ldots, N_1 - 1$,$k_2 = 1, 2, \ldots, N_2 - 1$ compute

$$Y_{fs}(k_1, k_2) = c_{T,3d,fit}(n = max(k_1, k_2)/2) \cdot Y_{fs}(k_1, k_2)\,, \tag{4.40}$$

with $c_{T,3d,fit}$ according to Equation (4.28).

- Compute the inverse discrete cosine transform y_{fs} of Y_{fs} according to Equation (4.34).

- To get the final frontside surface shape set $y_{fs} = -y_{fs}$.

To illustrate this method with an example we use as input y_{bs} as shown in Figure 17 (a). The results for y_{fs} and Y_{fs} at $U = 2000$ V are plotted in Figures 17 (b) and 18 (b). It can be observed how high spatial frequencies are damped out.

4.4 FEA of 3D Real E-Chucking

In this section we outline the main properties of the finite element calculation of a two body three dimensional contact problem. It is remarkable that this simulation assumes stress free boundary edges at $x, z = \pm L/2$.

The chuck and reticle mesh is plotted in Figure 16. The properties have been assumed close to [3]. The chuck mesh is a simple Cartesian block with $20 \times 20 \times 3$ equi-sized 8-node hexahedral elements and overall dimension $156 \times 156 \times 22.6$ mm. Typical chucks are made of ceramics with a Poisson ratio $\nu = 0.2$ and elastic modulus $E = 380$ GPa. A finite deformation elastic Neohookean material model has been applied.

The reticle mesh is basically a Cartesian block with $50 \times 50 \times 3$ equi-sized 8-node hexahedral elements and overall dimension $152 \times 152 \times 6.35$ mm. The backside surface has

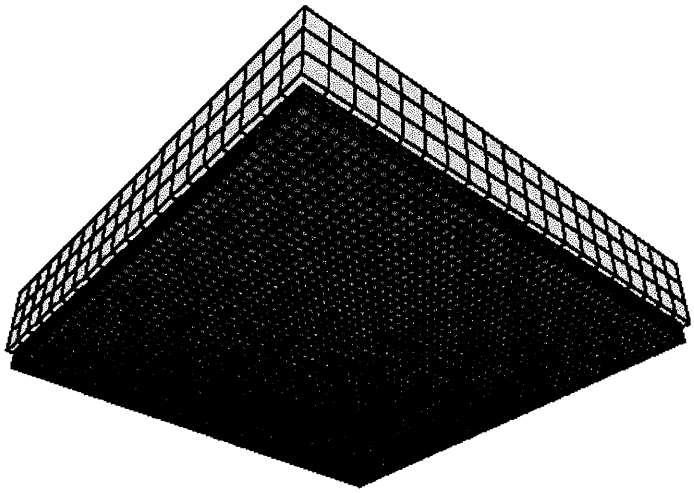

Figure 16: Finite element mesh of reticle (bottom) and chuck (top) for three dimensional analysis of real e-chucking.

been warped with a cubic B-spline function according to Appendix A. The curvature can be seen in Figure 17 (a) and is equivalent to the one chosen for the analytical analysis as discussed above. A finite deformation elastic Neohookean material model has been applied, with Poisson ratio $\nu = 0.17$ and elastic modulus $E = 67.6$ GPa.

The resulting flexural bending stiffness D can be estimated by classical plate theory as

$$D = \frac{Eh^3}{12(1-\nu^2)}. \tag{4.41}$$

For the chuck this results in 380 kNm and for the reticle in 1.5 kNm. Thus, when pressing the two objects together, the chuck surface can assumed to stay mostly undeformed.

The chuck is fixed in all three coordinate directions at selected points. In a first solution step the reticle is fixed at the frontside in all three coordinate directions and a displacement boundary condition on the frontside is applied, such that the contact can be established. In a second solution step the displacement boundary condition is removed and a pressure on the chuck surface facing the reticle backside and the reticle backside is applied. This pressure is computed and established in the contact driver in each solution iteration step as a function of the gap δ_a between chuck and reticle according to Equation (3.1). The fixed parameters ϵ_0, ϵ and δ_d are the same as discussed above and the voltage is set to $U = 2000$ V. A standard coulomb friction ($\mu = 0.2$) for the contact is chosen.

For the iterative solution of the nonlinear equations, the use of unsymmetric gradients and a line search is applied (see FEAP manual *'utan'*, [4]).

The result of the frontside displacement y_{feap} and the spectral components Y_{feap} of the reticle at chucking with 2000 V is illustrated in Figure 17 (c) and 18 (c) respectively.

4.5 Discussion

In order to predict the reticle frontside shape at a certain chucking voltage U, an analytical as well as a finite element calculation model have been developed. For illustration we took as input the spline surface as in Figure 17 (a) and assumed a chucking voltage $U = 2000$ V. Both results are plotted in Figure 17 (b) and (c), as well as in Figure 18 (b) and (c) for the spectral components.

It can be seen clearly that for each method high spatial frequencies ($k_1, k_2 > 10$) are not transmitted. This means that backside features with wavenumber greater than $n = 5$ are not expected to be observed at the chucked frontside for this example set of parameters.

For wavenumbers smaller than $n = 5$, however, there occurs a deviation between analytical prediction and finite element calculation (see Figure 18 (d)). Even if the overall shapes match pretty well (compare Figure 17 (b) and (c)), there is a deviation of average ~ 50 nm as can be seen in Figure 17 (d).

It is remarkable that the finite element calculation of this example took several hours, whereas the analytical computation was done in a few seconds. Improvements to the FEA solve time can possibly be achieved by utilizing a dynamic bandwidth optimizer to reduce changing fill patterns due to progressive contact. However this is an open question.

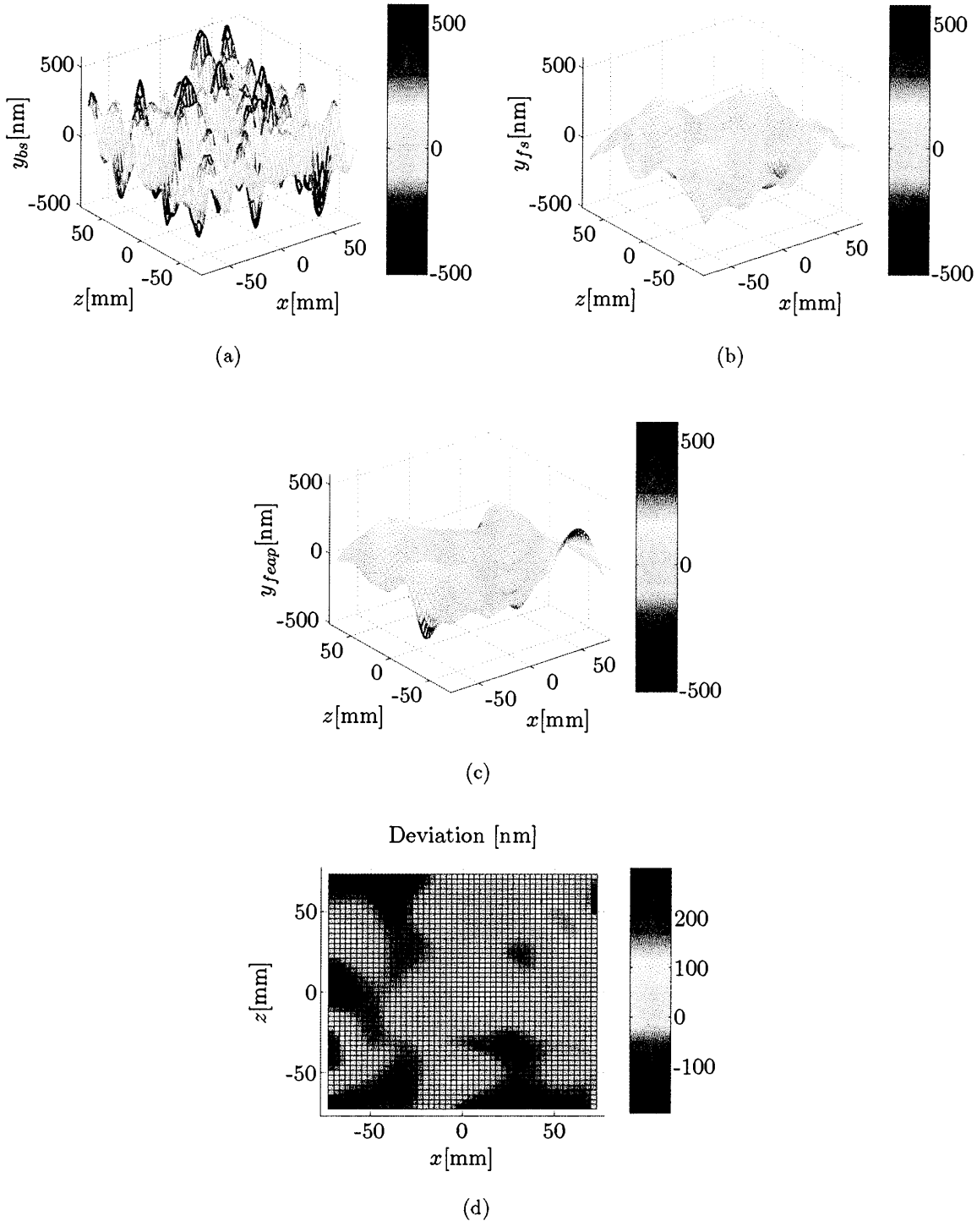

Figure 17: Example of three dimensional feature transfer, out-of-plane-distortion. (a) Reticle backsurface shape y_{bs} before e-chucking, (b) frontside shape y_{fs} according to analytical prediction of ideal e-chucking at voltage $U = 2000$ V, (c) FEAP simulation output y_{feap} of real e-chucking at voltage $U = 2000$ V, (d) absolute deviation between finite element and analytical computation, average = 51.149 [nm].

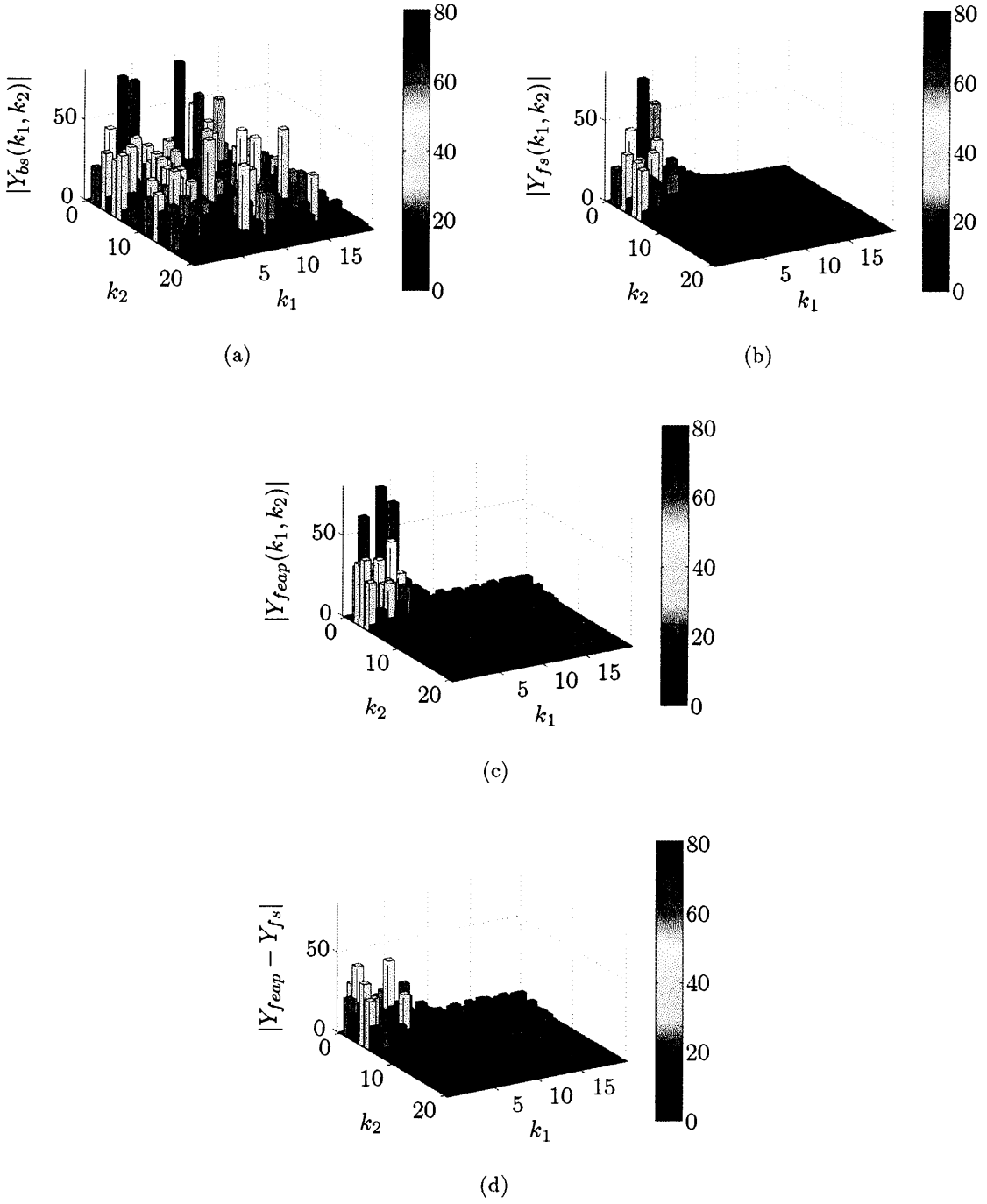

Figure 18: Example of three dimensional feature transfer, spectral perspective. (a) Spectral components of reticle backside pertubation Y_{bs} before e-chucking, (b) spectral components of frontside shape Y_{fs} according to analytical prediction of ideal e-chucking at voltage $U = 2000$ V, (c) discrete cosine transform of FEAP simulation output of real e-chucking Y_{feap} at voltage $U = 2000$ V, (d) absolute deviation between finite element and analytical computation.

5 Conclusion

This work provides an analytical approach as well as a finite element calculation to predict the transfer of reticle backside features to the frontside during electrostatic chucking at a certain voltage in two and three dimensions. The analytical solution is based on the assumption of an infinitely large reticle and periodic boundary conditions. A transmission coefficient has been derived which estimates the magnitude of a transmitted wavelength based on the solution of a linear elastic boundary value problem. A maximum allowable amplitude for a given wavelength has been calculated, which accounts for real chuck properties such as dielectric constant and applied voltage. A finite element calculation of real e-chucking with stress free boundaries has also been carried out.

For both, the two as well as the three dimensional case, an exemplary backsurface shape with high spatial frequency perturbation is used to illustrate and test the analytical against the finite element calculation. In order to handle such general surface shapes in the analytical approach, a discrete cosine transformation is used. For both methods it can be observed that small wavelengths cannot be seen at the frontside after chucking. This is in good agreement with the theoretical results. The overall shape can be estimated quite well, however there is deviation due to differences in low frequency transmission prediction. For our example set of parameters it has been observed that wavenumbers smaller than five are important to represent the reticle curvature. This observation might be used in the future to develop finite element calculations that only account for mesh perturbations with small wavenumbers. This would allow for a minimum number of elements and thus a remarkable speed-up in comparison to a one-to-one mesh of a backside surface shape with sharp edges, respectively high wavenumbers.

It is remarkable that the analytical solution is based on the assumption of an infinitely large reticle whereas the finite element calculation has stress free boundaries. This might explain the difference in the prediction of small wavenumber transmission. It has been shown that edge effects are not negligible for the ideal flattening case where we applied a cosine load on one reticle side. Future work might therefore bring out a better understanding of analytical real e-chucking, especially an understanding of the coupled contact and electrostatic forces, as well as the solution to the elasticity problem with stress free boundaries.

A Cubic B-Splines

In order to construct a random backsurface shape of the reticle we used a spline approximation of randomly generated numbers in Matlab. We briefly outline in this appendix the mathematical description of cubic B-splines in one and two dimensions. For the finite element analysis done as verification of the analytical prediction, this spline function has been used to develop a user mesh-manipulation subroutine in FEAP to generate the mesh.

A.1 Cubic B-Splines in 1 D

B-splines of higher order can be derived recursively from B-splines of lower order (see for example [2]). We first need to define a set of knots t_i with the help of coordinates $\tilde{x}_i$. Let us consider the set:

$$\begin{aligned}&\{t_0, t_1, t_2, t_3, t_4, t_5, ..., t_p, t_{p+1}, t_{p+2}, t_{p+3}, t_{p+4}\} := \\ &\{\tilde{x}_0, \tilde{x}_0, \tilde{x}_0, \tilde{x}_0, \tilde{x}_2, \tilde{x}_3, ..., \tilde{x}_{p-2}, \tilde{x}_p, \tilde{x}_p, \tilde{x}_p, \tilde{x}_p\}\,.\end{aligned} \tag{A.1}$$

Then B-splines of order 0 can be defined as

$$B_{i,0}(x) = \left\{ \begin{array}{ll} 1 & \text{if } t_i \le x < t_{i+1} \\ 1 & \text{if } x = t_{i+1} = x_p \\ 0 & \text{else} \end{array} \right\}, i = 0, 1, \ldots, p+3 \tag{A.2}$$

and $B_{i,0}(x) \equiv 0$, if $t_i = t_{i+1}$. B-splines of higher order are computed recursively: [1]

$$B_{i,\kappa}(x) = \frac{x - t_i}{t_{i+\kappa} - t_i} B_{i,\kappa-1}(x) + \frac{t_{i+\kappa+1} - x}{t_{i+\kappa+1} - t_{i+1}} B_{i+1,\kappa-1}(x). \tag{A.3}$$

For cubic B-splines one sets the order $\kappa = 3$.

A.2 Approximation

We now want to approximate a curve from which we know m function values f_j at given points x_j, $j = 1, 2, \ldots, m$. Let us define the spline approximation

$$s(x) = \sum_{i=0}^{p} \alpha_i B_{i,3}(x) \tag{A.4}$$

with coefficients α_i. This gives us an ansatz with $p+1$ degrees of freedom. If $m > p+1$, we need to apply the least-square method to compute the coefficients α_i.

$$\sum_{j=0}^{m} \left(s(x_j) - f_j\right)^2 \to \min_{\alpha_i}. \tag{A.5}$$

[1] Terms with denominator 0 are omitted.

A.3 Cubic B-Spline Approximation in 2 D

In order to present a surface in three space dimensions, the starting point of a spline approximation is a table with data

$$(x_j, z_j, f_j), j = 1, 2, \ldots, m. \tag{A.6}$$

Then one needs to search for a function

$$S(x, z) := \sum_{\nu=1}^{p} \sum_{\mu=1}^{l} c_{\nu\mu} B_{\mu,3}(x) B_{\nu,3}(z) \tag{A.7}$$

with $pl < m$ and

$$\sum_{j=1}^{m} \left(S(x_j, z_j) - f_j\right)^2 \to \min_{c_{\nu\mu}} . \tag{A.8}$$

For implementation, the corresponding equation system can be arranged in the following way:

$$\mathbf{B}\mathbf{c} = \mathbf{f}\,, \tag{A.9}$$

respectively

$$\begin{pmatrix} B_{1,3}(x_1)B_{1,3}(z_1) & B_{1,3}(x_1)B_{2,3}(z_1) & \cdots & B_{p,3}(x_1)B_{l,3}(z_1) \\ B_{1,3}(x_2)B_{1,3}(z_2) & B_{1,3}(x_2)B_{2,3}(z_2) & \cdots & B_{p,3}(x_2)B_{l,3}(z_2) \\ \vdots & \vdots & & \vdots \\ B_{1,3}(x_m)B_{1,3}(z_m) & B_{1,3}(x_m)B_{2,3}(z_m) & \cdots & B_{p,3}(x_m)B_{l,3}(z_m) \end{pmatrix} \begin{pmatrix} c_{11} \\ c_{12} \\ \vdots \\ c_{1l} \\ c_{21} \\ c_{22} \\ \vdots \\ \vdots \\ c_{pl} \end{pmatrix} = \begin{pmatrix} f_1 \\ f_2 \\ \vdots \\ f_m \end{pmatrix} .$$

The matrix $\mathbf{B}$ has dimension $(m \times pl)$. The coefficient vector $\mathbf{c}$ has dimension $(pl \times 1)$ and the data vector $\mathbf{f}$ has dimension $(m \times 1)$.

A.4 Example of a Spline Surface in Three Dimensions

In the analytical as well as the finite element calculation we use one and the same numerical example of a spline surface for comparison. Basically it has been obtained by fitting $m = 101^2$ randomly generated numbers f_j between -0.5 and 0.5 in Matlab assuming data location (x_j, z_j) at an equidistant mesh in the range $[-76, 76] \times [-76, 76]$. The spline properties are as follows: Take $p = l = 17$ and choose an equidistant mesh to generate knots as in Equation (A.1), where $\tilde{x}_0 = -76$ and $\tilde{x}_p = 76$. The result evaluated at FEAP nodal coordinates can be seen in Figure 17 (a).

Glossary

E-Chucking
Electrostatic chucking, the process where the reticle is clamped on a chuck due to the forces resulting from an electrical field., 2

Ideal E-Chucking
The model of electrostatic chucking with the assumption of an infinitely large reticle and idealization of contact forces. An analytical description has been carried out based on the results of ideal flattening., 16

Real E-Chucking
The more realistic model of a finite reticle, contact forces resulting from a two-body interaction and effective electrostatic forces. Solution has been determined using the finite element method in two and three dimensions., 22

Ideal Flattening
The mechanical boundary value problem for the reticle when applying a cosine load on the backside surface. An exact analytical solution in two dimensions as well as an approximation via energy minimization in two and three dimensions is derived., 6

Maximum Allowable Backside Amplitude
The maximum allowable amplitude, $\bar{u}_{bs}$, of a harmonic backside feature that can be flattened out at ideal e-chucking., 18

Transmission Coefficient
The amount of reduction in the frontside amplitude of a harmonic feature transmitted from the backside for ideal flattening, respectively ideal e-chucking., 9

References

[1] I. V. Andrianov and J. Awrejcewicz. Compatibility equations in the theory of elasticity. *Journal of Vibration and Acoustics*, 125:244–245, 2003.

[2] H.R. Schwarz and N. Köckler. *Numerische Mathematik*. B.G. Teubner Verlag, 6 edition, 2006.

[3] M. Nataraju, J. Sohn, S. Veeraraghavan, A. R. Mikkelson, K. T. Turner, and R. L. Engelstad. Electrostatic chucking for extreme ultraviolet lithography: Simulations and experiments. *Journal of Vacuum Science and Technology B*, 24:2834–2839, 2006.

[4] R.L. Taylor. Feap - a finite element analysis program: User manual. `http://ce.berkeley.edu/feap`.

[5] S. Timoshenko and J. N. Goodier. *Theory of Elasticity*. McGraw-Hill, 1970.